Soft Matter

Statistical mechanics of a double-stranded rod model for DNA melting and elasticity

Journal:	*Soft Matter*
Manuscript ID	SM-ART-03-2020-000521.R2
Article Type:	Paper
Date Submitted by the Author:	19-Jul-2020
Complete List of Authors:	Singh, Jaspreet; University of Pennsylvania, Department of Mechanical Engineering and Applied Mechanics Purohit, Prashant; University of Pennsylvania, Department of Mechanical Engineering and Applied Mechanics; University of Pennsylvania

Soft Matter

ARTICLE TYPE

Cite this: DOI: 00.0000/xxxxxxxxxx

Statistical mechanics of a double-stranded rod model for DNA melting and elasticity

Jaspreet Singh*†, Prashant K. Purohit*

Received Date
Accepted Date

DOI: 00.0000/xxxxxxxxxx

The double-helical topology of DNA molecules observed at room temperature in the absence of any external loads can be disrupted by increasing the bath temperature or by applying tensile forces, leading to spontaneous strand separation known as DNA melting. Here, continuum mechanics of a 2D birod is combined with statistical mechanics to formulate a unified framework for studying both thermal melting and tensile force induced melting of double-stranded molecules: it predicts the variation of melting temperature with tensile load, provides a mechanics-based understanding of the cooperativity observed in melting transitions, and reveals an interplay between solution electrostatics and micromechanical deformations of DNA which manifests itself as an increase in the melting temperature with increasing ion concentration. This novel predictive framework sheds light on the micromechanical aspects of DNA melting and predicts trends that were observed experimentally or extracted phenomenologically using the Clayperon equation.

1 Introduction

Double-stranded DNA (dsDNA) consists of two helical sugar-phosphate backbones held together by complementary base pairing. DNA melting or DNA denaturation is the separation of dsDNA into two single strands (ssDNA). The transition can be triggered by increasing the bath temperature or by applying tensile loads on the molecule. DNA melting is important in various biological processes such as DNA replication and DNA transcription, and ultimately impacts gene-expression. The first step in gene expression is the transcription of DNA to mRNA—it initiates via localized DNA melting caused by the protein RNA polymerase[1]. DNA replication and repair also initiate via localized melting caused by DNA helicases[2,3]. Several experimental techniques[4–6] such as fluorescence microscopy, optical tweezers and calorimetry provide evidence for *in-vitro* DNA melting–both thermal and force-induced[7,8]. The transition of a single base pair from bound to melted state is impacted by neighbouring base pairs; if the neighbouring base pairs are melted, it has higher probability of melting–this property is known as cooperativity. Experiments suggest that the dsDNA→ssDNA transition is strongly cooperative[9,10]. This property manifests itself as a sudden melting transition resembling a first-order phase transition; the increase in inter-strand distance with temperature is sudden as opposed to a mere incremental linear thermal expansion. We illustrate this point in the appendix by a simple model which embodies the basic concept and outcomes of cooperativity.

Here, a double-stranded elastic rod model[11] is combined with statistical mechanics[12] to capture various characteristics of the melting transition. Although thermal melting of DNA has been studied extensively for some decades now[13,14], a mechanics-based model which simultaneously captures both temperature-driven and tensile force-driven melting is yet to be explored. The novelty in the model proposed here is three fold: i) it goes beyond the existing Clausius-Clayperon based phenomenological description and provides a unified statistical-mechanics based framework to explain both temperature-driven and force-driven strand separation, ii) the model provides a mechanical basis for cooperativity in the melting transition by relating it to the bending resistance of the base pairs, and iii) the model accounts for the dependence of the electrostatic energy on the mircromechanical deformation of the birod which ultimately leads to familiar trends in melting temperature versus ion concentration and melting force versus ion concentration.

The sharp transition characterizing cooperative DNA melting depends on various factors[4] such as i) *the internal base pair sequence*: DNA fragments with higher GC content have higher melting temperatures, ii) *the tensile force*: experimental evidence suggests that the melting temperature decreases as the tensile load increases, and iii) *the ion concentration*: the melting force and melting temperature both increase with an increase in ion concentration. Most attempts to model the melting transition rely on using the Clausius-Clayperon equation to get empirical relations between the various quantities of interest such as melting temperature versus tensile force or over-stretching force versus

* *Department of Mechanical Engineering and Applied Mechanics, University of Pennsylvania, Philadelphia, USA. 19104*
† *Corresponding author. Email: singh1.3806@gmail.com*

the ion concentration *et cetera*[8,15]. Since these empirical models interface directly with the experimental data, they have superior predictive capabilities and produce experimentally verifiable predictions. However, this approach abstracts out the underlying mechanics and biochemistry driving the process. To circumvent this drawback to some extent, several statistical mechanics based models[16,17] have been proposed which begin by positing an energy functional that reproduces the characteristics of the cooperative melting transition observed experimentally. The detailed description sheds light on the underlying mechanism–cooperative H-bond disruption–and enables one to clearly discern the effect of various parameters such as, the cooperativity parameter and asymmetric interactions, on the melting transition. However, the inherent analytical intractability involved in evaluating the path integrals central to these approaches limits their application to relatively simple energy functionals. Molecular dynamics simulations have also been used to study several problems related to the melting transition, unzipping of DNA, and other structural transformations in DNA[18,19]. The interaction potentials are available for various chemical bonds in DNA thereby permitting a very detailed description of the structure, shape, and chemistry crucial to the problem. The results from the simulations agree well with the experimental data, but they entail a large computational burden.

Here, DNA is modelled as a 2D elastic birod. The elastic birod model has previously been used to study phenomenon such as allosteric interactions in DNA[20,21] where the double-helical geometry and micromechanical deformations of base pairs are important. In this paper, DNA is assumed to be a straight ladder-like birod for analytical tractability. We import ideas from statistical mechanics to show that the average distance between the two strands in a birod increases steeply in an unbounded fashion as the temperature reaches the melting point. A similar effect can be achieved by increasing the tensile load while keeping the temperature constant. A non-quadratic interaction between the strands is essential to achieve this effect. For a quadratic interaction, the equipartition theorem implies that the average change in the distance between the two strands is zero even as the temperature increases. Despite simplifying assumptions, the model presented here captures the key mechanical characteristics of DNA such as the entropic elasticity of long oligomers, the cooperative melting transition, and the effect of tensile force and ion concentration on melting.

The paper is organised as follows:

1. *Kinematics and energetics:* The section discusses the development of the model by highlighting key kinematic variables and their respective elastic constitutive relations.

2. *Force-extension curve:* The force-extension curve for a birod is computed and the key features of the entropic elasticity exhibited by the birod are demonstrated.

3. *Melting transition:* Temperature-driven and tensile force-driven melting transitions are discussed in detail. The focus is to quantitatively describe these transitions within the presented framework, and examine the interplay between the tensile force and the melting temperature.

4. *Effect of cooperativity:* The bending resistance of the base pairs is identified to be the cause of cooperativity observed in the melting transition. By varying only one parameter in the model, we are able to capture the experimental trends in both force- and temperature-driven melting transitions.

5. *Effect of ion concentration* The section uses the Poisson-Boltzmann formalism to compute the electrostatic energy for the birod. By accounting for the dependence of the electrostatic energy on the outer-radius of DNA in the birod model, it can be shown that both the melting temperature and melting force increase with ion concentration.

The model improves upon the existing statistical mechanics approaches[16,17] by computing (as opposed to positing) the energy functional from the kinematic description of the birod, so that the key features – temperature-induced melting, force-induced melting and the cooperativity – emerge naturally.

2 Kinematics and energetics

We closely follow the birod framework presented in Moakher and Maddocks[11]. We envision a straight ladder-like birod acted upon by an external force F as shown in fig.1. We assume small displacements throughout and confine ourselves to deformations in a plane. The two outer strands and the web connecting them are

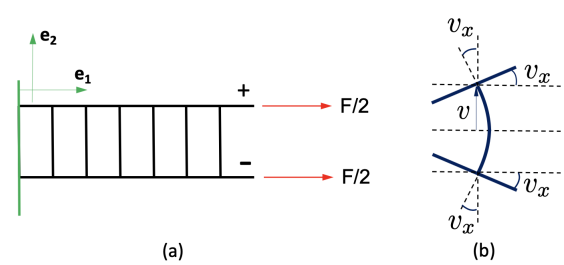

Fig. 1 (a) Cartoon of a straight birod acted upon by identical forces on both the strands. The two strands are referred to as $\pm$ strands. (b) Attachment of base pairs to the outer-strands. The short web representing the base pairs is welded to the outer strands.

elastic. The birod lies in $\mathbf{e}_1 - \mathbf{e}_2$ plane as shown in fig.1. The axial coordinate x is along $\mathbf{e}_1$: $x \in [0, L]$ where L is the contour length. The reference configuration of the $\pm$ outer strands denoted by $\mathbf{r}_0^{\pm}$ is

$$\mathbf{r}_0^{\pm} = x\mathbf{e}_1 \pm a\mathbf{e}_2. \tag{1}$$

For a general 2-D deformation in the $\mathbf{e}_1 - \mathbf{e}_2$ plane, the deformed configuration of the strands is:

$$\mathbf{r}^{\pm} = \int_0^x (1+\zeta)\mathbf{d}_1 \, dx \pm (a+v)\mathbf{d}_2 \pm u\mathbf{d}_1, \tag{2}$$

where, $\mathbf{d}_1 = \cos\theta\mathbf{e}_1 + \sin\theta\mathbf{e}_2$, and $\mathbf{d}_2 = -\sin\theta\mathbf{e}_1 + \cos\theta\mathbf{e}_2$. Note that $\mathbf{r} = \frac{\mathbf{r}^+ + \mathbf{r}^-}{2} = \int_0^x (1+\zeta)\mathbf{d}_1 \, dx$ denotes the deformed

centerline (global/macro displacement), while u and v denote the displacements of the $\pm$ strands relative to the centerline (micro-displacements). They are related to the shearing and stretching of the base pairs, respectively. In the entire paper, we use a small strain assumption[22] together with a moderate rotation approximation[23,24] which means: $\theta^2, v, \theta_x \sim O(\varepsilon)$, which implies $\cos\theta \sim 1 - \frac{\theta^2}{2}$ and $\sin\theta \sim \theta$. Any terms higher than $O(\varepsilon)$ such as $v\theta_x$, $\theta\theta_x$, and $u\theta_x$ are neglected. The moderate rotation hypothesis is applicable when the applied force is large, which is indeed the case for DNA melting.

Heretofore, $()_x$ denotes derivative w.r.t x. Hence, $\mathbf{d}_{1x} = \theta_x \mathbf{d}_2$ and $\mathbf{d}_{2x} = -\theta_x \mathbf{d}_1$. Now, $\mathbf{r}_x^{\pm} = (1 + \zeta \pm u_x \mp a\theta_x)\mathbf{d}_1 \pm v_x \mathbf{d}_2$. We assume that the outer strands are inextensible which implies $|\mathbf{r}_x^{\pm}| = 1$. Hence, $\zeta \pm u_x \mp a\theta_x = 0$, which gives $\zeta = 0$, and $u_x = a\theta_x$. Or, $u = a\theta$. For the $\pm$ strands, the tangent is $\mathbf{t}^{\pm} = \mathbf{d}_1 \pm v_x \mathbf{d}_2$, so the curvature is $\kappa^{\pm} = |\mathbf{t}_x^{\pm}| = \theta_x \pm v_{xx}$, respectively.

We now focus on the stretching, shearing and bending of the base pairs. Here we assume that the small rods–representing the base pairs–are welded to the outer long strands–representing the phosphate backbones (fig.1(b)). Such an arrangement permits the base pairs to exert both force and bending moment on the strands. For DNA, the base pairs are stacked on top of each other in a regular fashion, the space constraints and repulsion from neighbouring bases in this crowded environment prevents the bases from moving freely. A simplistic approach is to penalize the relative motions of the bases via elastic bending and stretching potentials, as done in this paper. This approach is similar to several previous studies[25–28] where elasticity of base pairs has been shown to play an important role. A detailed study regarding the actual nature of the bonds is beyond the scope of the current work

As mentioned, the tangent vectors to the $\pm$ strands are $\mathbf{t}^{\pm} = \mathbf{d}_1 \pm v_x \mathbf{d}_2$, hence the respective normal vectors are $\mathbf{n}^{\pm} = \mp v_x \mathbf{d}_1 + \mathbf{d}_2$. The rotation matrices $\mathbf{Q}^{\pm} = [\mathbf{t}^{\pm}, \mathbf{n}^{\pm}]$ can be decomposed as,

$$\mathbf{Q}^{\pm} = \begin{bmatrix} \cos\theta & -\sin\theta \\ \sin\theta & \cos\theta \end{bmatrix} \begin{bmatrix} 1 & \mp v_x \\ \pm v_x & 1 \end{bmatrix}. \tag{3}$$

$\mathbf{Z} = \begin{bmatrix} \cos\theta & -\sin\theta \\ \sin\theta & \cos\theta \end{bmatrix}$ depends on the deformation of the centerline, while $\begin{bmatrix} 1 & \mp v_x \\ \pm v_x & 1 \end{bmatrix}$ depends only on the displacements of the strands about the center-line. $\mathbf{Q}^{\pm}$ can be used to compute the micro-rotation tensor $\mathbf{P}$ and macro-rotation tensor $\mathbf{Q}$ (for details see[11]).

$$\mathbf{P}^2 = \mathbf{Q}^{+}\mathbf{Q}^{-T} = \mathbf{Z}\Big(\mathbf{I}_{2\times 2} + \begin{bmatrix} 0 & -2v_x \\ 2v_x & 0 \end{bmatrix}\Big)\mathbf{Z}^T, \tag{4}$$

where $\mathbf{I}_{2\times 2}$ is the identity tensor. Hence,

$$\mathbf{P} = \begin{bmatrix} 1 & -v_x \\ v_x & 1 \end{bmatrix}, \tag{5}$$

and

$$\mathbf{Q} = \mathbf{P}\mathbf{Q}^{-} = \mathbf{Z} = \mathbf{d}_1 \otimes \mathbf{e}_1 + \mathbf{d}_2 \otimes \mathbf{e}_2. \tag{6}$$

The stretching and shearing of the base pairs are proportional to $\xi = \mathbf{Q}^T\mathbf{w} - \mathbf{w}_0$[11], where $\mathbf{w} = \frac{\mathbf{r}^+ - \mathbf{r}^-}{2}$, $\mathbf{w}_0 = \frac{\mathbf{r}_0^+ - \mathbf{r}_0^-}{2}$, and $\xi = a\theta\mathbf{e}_1 + v\mathbf{e}_2$.

Just like the stretching and shearing of the base pairs can be computed from the difference in the displacements of the outer-strands, the bending of the base pairs can be computed from the rotations on the $+$ and $-$ strand. In fact, the moment transferred by the web is proportional to the Gibbs vector of the micro-rotation tensor $\mathbf{P}$[11]. In a 2D-setting, this moment can be easily computed; since the directions of the rotations are fixed, there is no twisting, and bending is proportional to v_x (see fig.1(b) for details).

We now discuss the energy associated with each kinematic deviation from the reference configuration. The bending energy per unit length for the outer $\pm$ strands is $E_s = \frac{EI}{2}(\kappa^{+2} + \kappa^{-2}) = EI(\theta_x^2 + v_{xx}^2)$ where EI is the bending resistance of the outer strands. The energy associated with shearing the base pairs is $E_{sh} = L_1 a^2 \theta^2$, where L_1 is the associated elastic constant. For the stretching of the base pairs, we use an assymetric energy profile of the form $f(x) = (e^{-\lambda x} - 1)^2$– known as the Morse potential. This approach is meant to penalize the steric hindrance between the two strands and has been previously used in literature[16,17]. Hence, the energy per unit length required to stretch the base pairs $E_{st} = L_2(e^{-\lambda v} - 1)^2$. The energy associated with the bending of the base pairs is $E_{bb} = H_1 v_x^2$. Altogether, the energy of the birod is,

$$\begin{aligned} E_e &= \int_0^L dx\ \big(E_b + E_{sh} + E_{st} + E_{bb}\big) \\ &= \int_0^L dx\ \big(EI(\theta_x^2 + v_{xx}^2) + L_1 a^2\theta^2 + L_2(e^{-\lambda v} - 1)^2 + H_1 v_x^2\big), \end{aligned} \tag{7}$$

where both v and θ are functions of x. This energy will enter the statistical mechanical model for the birod. We use the following values of elastic constants: $EI = 0.15\ pNnm^2$, $L_1 = 80\ pN/nm^2$, $L_2 = 1280\ pN/nm^2$, $H_1 = 0.33\ pN$, $a = 1\ nm$, and $\lambda = 0.5\text{Å}^{-1}$. The values of the constants were chosen in a way that melting temperature of DNA at zero tensile force is approximately 75°C (fig. 3 of the main text). Also, the constants were tweaked to get the variation of the melting temperature with tensile force in the right region (fig.5(c) of the main text). One could use other criteria as well, such as the persistence length of B-DNA at room temperature and stretch moduli of B-DNA *et cetera*. However, the experimental values are for a 3D helical DNA which might not give the correct melting temperature in our model. Since, the focus here is on the melting of DNA, we chose to stick to the former.

3 Force-extension curve for a thermally fluctuating birod

In this section, we discuss the force-displacement curve for the ladder-like birod. We already have the elastic energy of the birod given by eqn. 7. Next we need to compute the work done by external force F distributed equally on both strands. For $+$ strand, the displacement at the free end is,

$$\begin{aligned}\Delta^+ &= \int_0^L (\mathbf{t}^+.\mathbf{e}_1 - 1)\, dx \\ &= \int_0^L (\cos\theta - \sin\theta\ v_x - 1)\, dx = \int_0^L (-\frac{\theta^2}{2} - \theta v_x)\, dx.\end{aligned} \tag{8}$$

Similarly, for $-$ strand, $\Delta^- = \int_0^L \mathbf{t}^-.\mathbf{e}_1\, dx - L$, which upon simplification yields $\Delta^- = \int_0^L (-\frac{\theta^2}{2} + \theta v_x)\, dx$. Summing up the individual contributions from the strands yields,

$$W_e = \frac{F}{2}(\Delta^+ + \Delta^-) = F\int_0^L -\frac{\theta^2}{2}\, dx. \tag{9}$$

Hence, the potential energy functional of the birod is,

$$\begin{aligned}E =& E_e - W_e = E(\theta(x), v(x)) \\ =& \int_0^L dx\ \big(EI(\theta_x^2 + v_{xx}^2) + L_1 a^2\theta^2 + L_2(e^{-\lambda v} - 1)^2 + H_1 v_x^2 + \frac{F}{2}\theta^2\big).\end{aligned} \tag{10}$$

The average end-to-end extension is,

$$y = \int_0^L \cos\theta\ dx \approx \int_0^L \Big(1 - \frac{\theta^2}{2}\Big)\, dx, \tag{11}$$

where we assumed that θ is a moderate rotation. The average end-to-end distance $\langle y\rangle$ is,

$$\langle y\rangle = L - \langle \int_0^L \frac{\theta^2}{2}\, dx\rangle, \tag{12}$$

where $\langle\rangle$ denotes the ensemble average. We need to evaluate the partition function to compute the above average. The partition function of the birod is a path-integral given as follows,

$$Z = \int \mathscr{D}\theta(x) \int \mathscr{D}v(x)\ \exp(-\frac{E(\theta(x), v(x))}{k_B T}). \tag{13}$$

The above partition function Z can be multiplicatively decomposed: $Z = Z_v Z_\theta$, where Z_v comprises the path-integral over the function $v(x)$, while Z_θ over $\theta(x)$.

$$Z_\theta = \int \mathscr{D}\theta(x)\ \exp(-\frac{E_\theta}{k_B T}), \quad \text{and} \quad Z_v = \int \mathscr{D}v(x)\ \exp(-\frac{E_v}{k_B T}), \tag{14}$$

where,

$$\begin{aligned}E_\theta &= \int_0^L dx\ \big(EI\theta_x^2 + (L_1 a^2 + \frac{F}{2})\theta^2\big), \quad \text{and} \\ E_v &= \int_0^L dx\ \big(EI v_{xx}^2 + L_2(e^{-\lambda v} - 1)^2 + H_1 v_x^2\big).\end{aligned} \tag{15}$$

Now,

$$\langle \int_0^L \frac{\theta^2}{2}\, dx\rangle = \frac{1}{Z}\int \mathscr{D}\theta(x) \int \mathscr{D}v(x)\ \Big(\int_0^L \frac{\theta^2}{2}\, dx\Big)\ \exp(-\frac{E(\theta(x), v(x))}{k_B T}). \tag{16}$$

Summing over all the admissible functions $v(x)$ and canceling the common factor Z_v yields,

$$\langle \int_0^L \frac{\theta^2}{2}\, dx\rangle = \frac{1}{Z_\theta}\int \mathscr{D}\theta(x)\Big(\int_0^L \frac{\theta^2}{2}\, dx\Big)\ \exp(-\frac{E_\theta(\theta(x))}{k_B T}), \tag{17}$$

The above expression can be evaluated by differentiating the logarithm of the partition function.

$$\langle \int_0^L \frac{\theta^2}{2}\, dx\rangle = -k_B T\frac{\partial \ln Z_\theta}{\partial F}, \tag{18}$$

which gives,

$$\langle y\rangle = L + k_B T\frac{\partial \ln Z_\theta}{\partial F}. \tag{19}$$

Notice that the remaining functional is only a function of $\theta(x)$. Following Su and Purohit[29], we discretize the domain $x \in [0, L]$ into $n-$segments $(x_i, x_{i+1}]$, where $0 \le i \le n$, such that $\theta_x = \frac{\theta_i - \theta_{i-1}}{\delta}$ where $\delta = \frac{L}{n}$. For the energy functional E_θ, the integral over the domain can be expressed as a quadratic expression in terms of θ_i's:

$$\begin{aligned}E_\theta^n &= \sum_{i=0}^n \delta\Big[EI\Big(\frac{\theta_i - \theta_{i-1}}{\delta}\Big)^2 + L_1 a^2\theta_i^2 + \frac{F}{2}\theta_i^2\Big] \\ &= \theta.\Big[\frac{EI}{\delta}\mathbf{A} + \delta(L_1 a^2 + \frac{F}{2}\mathbf{I})\Big]\theta = \theta.\mathbf{K}_\theta\theta,\end{aligned} \tag{20}$$

where $\theta = [\theta_0, \theta_2, ...\theta_n]^T$, $\mathbf{I}$ is an identity matrix, and $\mathbf{A}$ is another matrix as follows:

$$\mathbf{A}_{n\times n} = \begin{bmatrix} 1 & -1 & 0 & 0 & 0 & \dots & 0 \\ -1 & 2 & -1 & 0 & 0 & \dots & 0 \\ 0 & -1 & 2 & -1 & 0 & \dots & 0 \\ \vdots & & & \ddots & & & \vdots \\ 0 & 0 & \dots & 0 & -1 & 2 & -1 \\ 0 & 0 & \dots & 0 & 0 & -1 & 1 \end{bmatrix}.$$

Notice that $\mathbf{K}_\theta$ is a constant depending only on the elastic properties of the birod. This enables us to transform the path integral Z_θ into a $n-$dimensional integral as follows:

$$\begin{aligned}Z_\theta^n &= \int \mathscr{D}\theta(x)\exp(-\frac{E_\theta}{k_B T}) \\ &= \prod_{i=0}^n \Big(\int_{-\pi}^{\pi} d\theta_i\Big)\exp(-\frac{E_\theta^n}{k_B T}) = \int d\theta\ \exp(-\frac{\theta.\mathbf{K}_\theta\theta}{k_B T}).\end{aligned} \tag{21}$$

To evaluate the above integral conveniently, we change the limits from $-\pi, \pi$ to $-\infty, \infty$, which transforms the above expression into a $n-$dimensional Gaussian integral which can be computed

analytically as follows,

$$Z_\theta^n = \int_{(-\infty,\infty)^{n+1}} d\theta \ \exp(-\frac{\theta.\mathbf{K}_\theta\theta}{k_BT}) = \pi^{n/2}\frac{(k_BT)^{n/2}}{\sqrt{\det \mathbf{K}_\theta}}. \quad (22)$$

Substituting it in eqn. 19 gives,

$$\langle y\rangle = L + k_BT\frac{\partial \ln Z_\theta}{\partial F} = L - \frac{k_BT}{2}\frac{\partial \log\det \mathbf{K}_\theta}{\partial F}. \quad (23)$$

An analytical derivation based on Fourier integral techniques[30,31] is presented in appendix A2. The plot for the force-extension relation for the birod is shown in fig.2(a). At large forces ($F > 20$ pN), it can be approximated by a WLC model[32] with persistence length 100 nm. As shown in fig. 2 (b), the end-to-end distance decreases with an increase in temperature–a typical entropic elasticity characteristic. The decrease in the variance of the transverse displacement ($w(x) = \int_0^x \sin\theta \ dx$) with an increase in tensile force shown in fig. 2 (c) is yet another signature of entropic elasticity[31] (For analytical expression of $\langle w^2\rangle$ see Purohit *et al.*[31]).

4 Thermal melting

At room temperature under zero tensile loads, the DNA molecule exhibits a double-helical structure. However, as the temperature increases and reaches the melting temperature, the complementary base pairing is disrupted and the two strands spontaneously disintegrate into two single strands. This melting transition is highly cooperative[33], and the temperature at which it occurs is referred to as the melting temperature. Aside from the sequence dependence, the melting temperature is also highly sensitive to the tensile loads and the ionic concentration of the solution[8,15]. Experimental evidence suggests that the melting temperature increases with the increase in ionic concentration and drops with the increase in tensile loads on the molecule. Thermodynamics based studies relying on Clausius-Clayperon equation have led to various empirical relations among these quantities[8,15,33]. To provide a rough idea about the melting temperature, for the Na^+ concentration of 0.075 M, the melting temperature is approximately $75°C$[34] (see reference for the exact bp-sequence). Using the birod model, we seek a relation between the average inter-strand distance $\langle v\rangle$ and the temperature T. In this section, we assume no tensile forces on the molecule, hence the elastic potential energy functional E is,

$$E = \int_0^L dx \ \left(EI(\theta_x^2 + v_{xx}^2) + L_1a^2\theta^2 + L_2(e^{-\lambda v} - 1)^2 + H_1 v_x^2\right). \quad (24)$$

The average distance between the strands can be computed as follows:

$$\langle v\rangle = \frac{1}{Z}\int \mathscr{D}\theta(x)\int \mathscr{D}v(x) \ \left(\frac{1}{L}\int_0^L v(x)dx\right) \ \exp(-\frac{E(\theta(x), v(x))}{k_BT}), \quad (25)$$

where the expression for the energy E and the partition function Z can be found in eqn. 7 and eqn.13, respectively. As done in the previous section, we discretize the domain into n-elements which transforms the integrals into sums and the path integrals into n-dimensional integrals:

$$\begin{aligned} E^n &= \sum_{i=0}^n \delta\Big[EI\Big(\frac{(\theta_i - \theta_{i-1})^2}{\delta^2} + \frac{(v_{i+1} - 2v_i + v_{i-1})^2}{\delta^4}\Big) \\ &\quad + L_1a^2\theta_i^2 + L_2(e^{-\lambda v_i} - 1)^2 + H_1\frac{(v_i - v_{i-1})^2}{\delta^2}\Big], \\ Z^n &= \prod_{i=0}^n \Big(\int_{(-\infty,\infty)^2} d\theta_i dv_i\Big)\exp(-\frac{E^n}{k_BT}), \\ \langle v\rangle &= \frac{1}{Z^n}\prod_{i=0}^n \Big(\int_{(-\infty,\infty)^2} d\theta_i dv_i\Big)\Big(\frac{1}{n}\sum v_i\Big)\exp(-\frac{E^n}{k_BT}). \end{aligned} \quad (26)$$

In contrast to the last section where the discretization together with quadratic energy functional enabled us to analytically evaluate the partition function, the partition function above can not be evaluated analytically because of the non-quadratic term $(e^{-\lambda v_i} - 1)^2$. Hence, we use Monte-Carlo simulations to compute $\langle v\rangle$ as a function of the bath temperature T. We use the Metropolis algorithm[35] to perform the MC simulations (for more details see appendix A3). The results are recorded in fig. 3. Each individual marker $\times$ is one simulation. We find that as the temperature increases the average inter-strand distance increases strongly in a nonlinear fashion, hence can not be alluded to as mere thermal expansion. The asymmetry in the nonlinear interaction term $((e^{-\lambda v} - 1)^2)$ is crucial for achieving this effect; if quadratic interaction is used the average inter-strand distance is zero even as the temperature increases.

We fit a continuous spline to $\langle v\rangle$ vs T data to indicate the trend. In reference configuration, the average inter-strand distance is 10 Å. We assume that the melting of a single discrete unit as shown in fig.3 occurs at 50% strain, *i.e.* when the unit is stretched to 15Å or when $v_i = 5$Å. The oligomer is considered melted when more than 50% of the units are melted. We plot the fraction of melted DNA $f_m = \frac{1}{n}\sum_{i=1}^n \mathbb{I}(v_i > 5\text{Å})$, where $\mathbb{I}(v_i > 5\text{Å}) = 1$ if $v_i > 5$Å and 0 otherwise, as a function of temperature T in the inset. The data for f_m vs T is fit using a logistic function $g(x) = \frac{1}{1+e^{-a_0(x-a_1)}}$ to read off the melting temperature from the plot: $T_m \approx 360$K, which is quite close to the results for dsDNA documented in literature[8,15,34]. The melted ($v_i > 5$Å) and unmelted ($v_i < 5$Å) units and the corresponding v_i are shown for $T = 250$K and $T = 425$K. The contiguous strands of unmelted DNA and melted DNA observed below and above the melting temperature, respectively, indicate cooperative interactions. Although the melting criterion $v_i = 5$Å was deliberately chosen so that the results from the model agree with the experimental data, our main message is that the birod model has the essential ingredients to account for the cooperative melting transition and these crucial factors emerge naturally from the kinematic description of the birod.

5 Tensile force-induced melting

In this section, the effect of tensile force on the melting temperature is explored. We consider the birod shown in fig.4. Here, we apply the force on one strand as previous studies[36] have indicated. As before, we need to compute the potential energy of

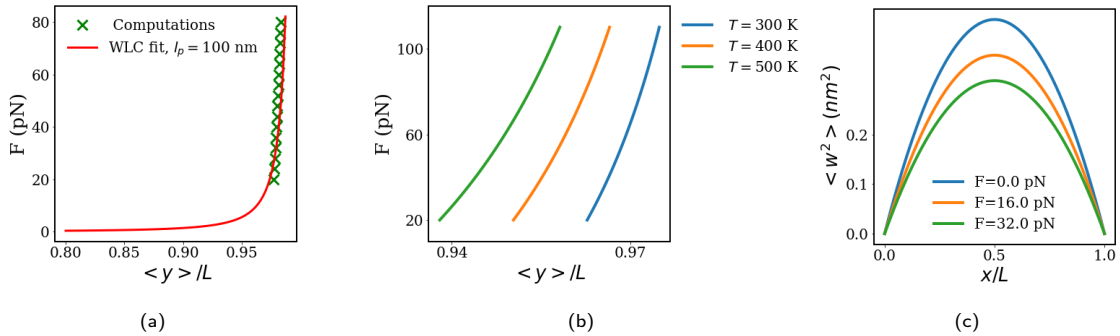

(a) (b) (c)

Fig. 2 (a) For large force, force-extension curve of the birod is similar to a WLC model with a persistence length of $l_p = 100$ nm. (b) Effect of increase in temperature on the force-extension curve is in agreement with expectations of entropic elasticity. (c) $\langle w^2 \rangle$ vs x for various values of tensile force F. The boundary conditions for (a) and (b) are fixed-free while for (c) it is hinged-hinged. The values of parameters in the energy functional are $EI = 0.15\ pNnm^2$, $L_1 = 80\ pN/nm^2$, $L_2 = 1280\ pN/nm^2$, $H_1 = 0.33\ pN$, $a = 1\ nm$, and $\lambda = 0.5\text{Å}^{-1}$. For these calculations $L = 200$ nm and $n = 300$.

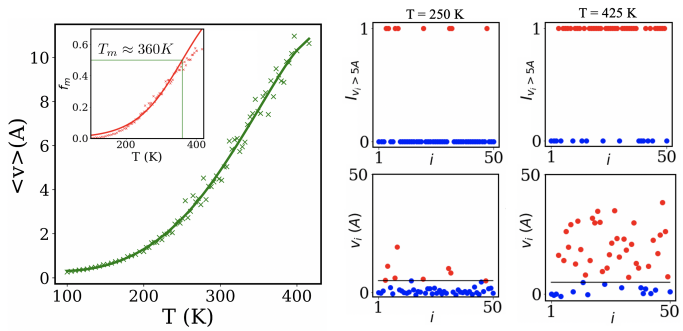

(a) (b) (c)

Fig. 3 (a) $\langle v \rangle$ vs T curve. Each green $\times$ marker is $\langle v \rangle$ computed from an individual MC simulation at that temperature, while the solid green line is a smoothed univariate spline curve plotted to indicate the trend. The inset shows the corresponding data for the melted fraction f_m, which is fit using a logistic function to compute the melting temperature ($T_m = 360$ K). (b) v_i and $I(v_i > 5\text{Å})$ vs i ($1 \le i \le n$) at $T = 425$ K. Red $\circ$ and blue $\circ$ markers denote the melted ($v_i > 5\text{Å}$) and unmelted ($v_i < 5\text{Å}$) discrete units at $T = 250$ K. The corresponding v_i are also shown; here the solid black line shows $v_i = 5\text{Å}$ for reference. (c) v_i and $I(v_i > 5\text{Å})$ at $T = 425$ K. The data in (b) and (c) are computed at the end of $N = 1000000$ MC steps. We observe contiguous strands of unmelted DNA below the melting temperature and melted DNA above the melting temperature, indicating cooperative interactions. Further details on MC simulations are given in appendix A3.

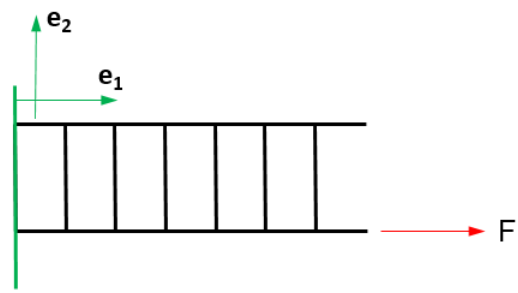

Fig. 4 The birod cartoon for studying DNA melting. Note that the force is applied only on one strand.

the birod in this configuration. The elastic energy of the birod is available in eqn.7. The work done by external force F is,

$$W_e = F \int_0^L dx\ (\mathbf{t}^- . \mathbf{e}_1 - 1). \tag{27}$$

Now, $\mathbf{t}^- = \mathbf{d}_1 - v_x \mathbf{d}_2$, hence $\mathbf{t}^- . \mathbf{e}_1 = \cos\theta + v_x \sin\theta \approx 1 - \theta^2/2 + v_x\theta$. This implies,

$$W_e = F \int_0^L dx\ (-\frac{\theta^2}{2} + v_x\theta). \tag{28}$$

The elastic potential energy E is,

$$\begin{aligned} E =& E_e - W_e \\ =& \int_0^L dx\ \big(EI(\theta_x^2 + v_{xx}^2) + (L_1 a^2 + \frac{F}{2})\theta^2 + \\ & L_2(e^{-\lambda v} - 1)^2 + H_1 v_x^2 - F v_x \theta\big). \end{aligned} \tag{29}$$

The term $F v_x \theta$ is responsible for coupling the force F and the inter-strand distance v. Now for a given $\theta(x)$, the probability of observing a configuration with interstand distance $v(x)$ at force F is $e^{F v_x \theta / k_B T}$ times the probability of observing the same configuration at $F = 0$. Granted, as the force F increases the birod straightens out and θ decreases as can be inferred from fig.2(b). However, for high forces (> 15 pN), the DNA molecule with a persistence length 50 nm is mostly straight. In other words, the $\theta(x)$ does not change much as the force increases from 15 pN to 40 pN, however this makes the higher values of $v(x)$ much more likely. Based upon this qualitative argument we expect that the melting temperature should decrease with an increase in tensile load F.

The $\langle v \rangle$ vs T curves are presented in fig.5(a) for various tensile forces F, and we indeed observe that for a given temperature, the inter-strand separation increases with increasing tensile loads. We use the same criteria for computing the melting temperature

T_m as in the previous section: the temperature at which the fraction of melted DNA f_m exceeds 0.5. We fit the f_m vs T data using a logistic function $g(x) = \frac{1}{1+e^{-a_0(x-a_1)}}$ as done previously to get the melting temperature T_m for various values of external load F. We find that T_m decreases with an increase in F as shown in fig.5(c). We use the experimental data from Zhang *et al*[4] to conclude that the trend is correct. The slope of the line depends on the elastic constants of the birod and for the values chosen here a quantitative match is also achieved.

Fig.5(d) shows that at a constant temperature ($T = 300$ K), the average inter-strand distance $\langle v \rangle$ increases with an increase in tensile load F indicating force-induced melting. We fit the simulation data using a smooth spline to highlight the trend. The corresponding melted fraction f_m vs tensile load F is plotted in the inset. The logistic function fitted to the data reveals that at $F = 40$ pN $f_m = 0.5$ *i.e.* DNA has melted. The critical force at which the DNA melts is sometimes referred to as *overstretching force*[15]. Experimental data shows that this force driven melting transition occurs at $F = 60$ pN[7,37] (for exact details regarding the pH, sequence dependence and salt concentration see references), hence the value predicted by our model is in the correct region. Note that we modelled DNA using a straight ladder-like birod instead of a helical one, and we restricted the formulation to planar deformations–these assumptions could be causing this deviation.

6 Effect of cooperativity parameter

The structural transition from dsDNA→ssDNA is known to be highly cooperative[33]. The cooperativity exerts a strong influence on the mechanical behavior such as determining the sharpness of the force-extension curves and influences the melting temperature and overstretching force. One phenomenological approach accounting for cooperativity comes from authors' previous work[38] in which interfacial energy among various phases of DNA makes the transition among them cooperative. Yet, another approach is to postulate an energy functional which includes terms proportional to the gradient of the inter-strand distance[16,17]. The motivation for such approaches comes from Cahn–Hilliard formulation[39] widely used to study nucleation and spoinodal decompositions in phase field modelling, where the phase boundaries are energetically penalized using a term proportional to the square of the gradient of the order parameter ($\sim (\nabla\phi)^2$). A similar idea for penalizing the gradients is also used in the Landau-Ginzburg approach[12] to study superfluidity and superconductivity transitions. In the birod formulation presented here, the gradient terms proportional to v_x^2 emerge from the bending rigidity of the base pairs which imparts cooperativity to the model. We demonstrate the effects and outcomes of cooperativity using a simple model in appendix A1.

We plot the fraction of melted DNA f_m versus the temperature T and tensile load F in fig. 6(a) and (b), respectively. As the bending resistance of base pairs (cooperativity parameter) H_1 increases, the melting temperature and overstretching force both increase. Experimental evidence documented in Zhang *et al*[4] shows that as the GC content of the molecule increases, so does the overstretching force and melting temperature. Higher values of H_1 represent higher GC content since GC base pairs consist of 3 hydrogen bonds compared to 2 hydrogen bonds in AT base pairs and are consequently stiffer. Higher GC content can have other effects such as increasing the constants L_1 and L_2 as well; we deal with this issue in appendix A4. In case of force-driven melting, the transition becomes sharper too. This is demonstrated by fitting the logistic function $g(x) = \frac{1}{1+e^{-a_0(x-a_1)}}$ to f_m vs F transitions and observing that the parameter a_0 which quantifies the width of the transition increases monotonically with H_1. The phenomenological evidence for the sharpening can be found in authors' previous work[38] in which higher interfacial energies representing higher cooperativity parameters (therefore higher H_1) correspond to sharper transitions.

7 Effect of ion concentration

Both force-induced and temperature-induced melting transitions are sensitive to the ion concentration of the solution. Here, the effect of changes of ion concentration on these melting transitions is explored. The phosphate backbone of DNA is negatively charged, hence the positive ions in the solution cluster around it. This stabilizes the double-stranded form of DNA. Therefore, the melting temperature and melting force should increase with an increase in ion concentration, as suggested by experimental evidence[4]. Empirical relations based on the Clausius-Clayperon equation connecting the melting force and melting temperature to the ion concentration have been proposed[8,40]. In this section we account for the effect of electrostatic interactions on the melting temperature and melting force by means of a Poisson-Boltzmanm equation based polyelectrolyte model of DNA[41].

We use a highly simplified 1D Poisson-Boltzman equation to describe the electrostatics. For a detailed description refer Frank-Kamenetskii et al.[41]. The purpose of what follows is to compute the electrostatic energy of the rod in a configuration described by $\theta(x)$, $v(x)$ and clearly highlight the underlying assumptions. To compute the electrostatic energy, we assume that the DNA molecule is almost straight *i.e.* the effect of $\theta(x)$ is negligible–a complete description of electrostatics for bent DNA is beyond the scope of the current study. Secondly, we assume that the radius of the DNA molecule in a configuration described by $v(x)$ is $a + v_a$, where $v_a = \frac{1}{L}\int_0^L v(x)dx$. This assumption transforms the 2D PDE into a 1D ODE. We consider only monovalent ions such as K^+ and Na^+. Within the scope of these assumptions, the boundary value problem for the electrostatic potential $U(y)$ can be written as,

$$\begin{aligned} \frac{d^2w}{dy^2} &= \chi^2 \sinh(w), \\ w'(a+v_a) &= \frac{2q}{a+v_a}, \quad w(R) \to 0 \quad \text{as} \quad R \to \infty. \end{aligned} \tag{30}$$

Here, y is the coordinate perpendicular to x in fig.1, $w = \frac{eU}{k_B T}$ is the nondimensional potential, e is the electronic charge, and $a + v_a$ is the average radius of the DNA helix. The dimensionless charge $q = \frac{l_B}{b}$, where $l_B = \frac{e^2}{Dk_B T}$ is the Bjerrum's length, b is the length of the cylinder containing negative charge e, ε_0 is vacuum

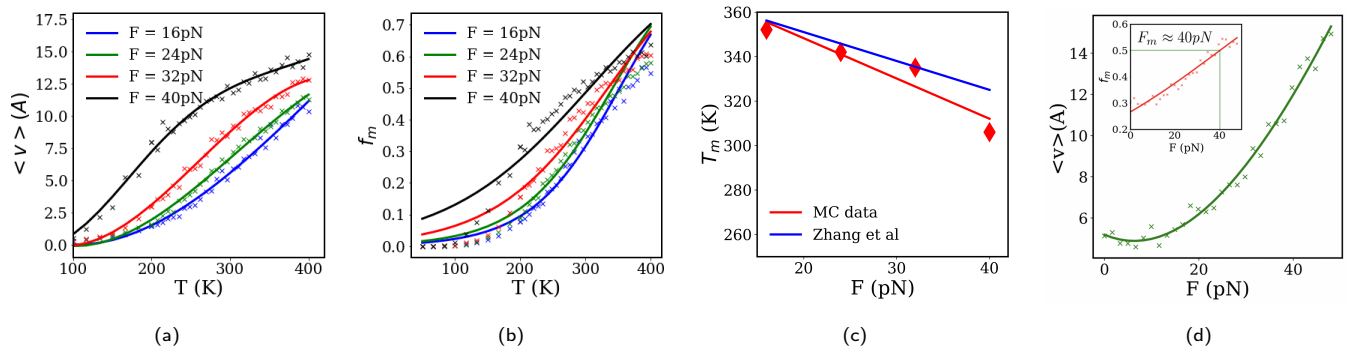

Fig. 5 (a) Average inter-strand distance $\langle v \rangle$ vs temperature T curves for different values of tensile force F. Here each marker $\times$ denotes one MC simulation and the solid lines are smooth splines being fit to the MC simulation data to indicate the trend. (b) Fraction of melted DNA f_m vs temperature T for different tensile loads. The MC simulation data is fitted using a logistic function to compute the melting temperature. (c) Melting temperature T_m vs tensile force F as computed from fig. (b). The experimental data is from[4]. (d) Average inter-strand distance $\langle v \rangle$ vs tensile force F ($\times$) at 300 K fitted using a smooth spline (solid line). The inset shows the corresponding melted fraction f_m ($\times$) fitted using a logistic function (solid line). $F \approx 40$ pN when $f_m = 0.5$.

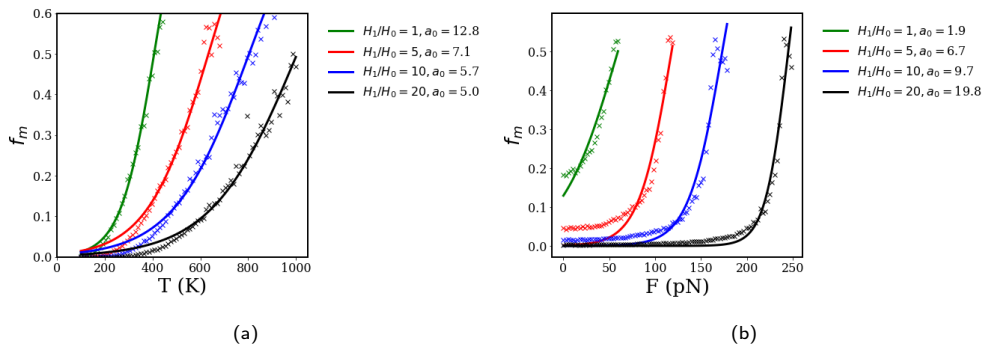

Fig. 6 (a) Effect of the cooperativity parameter H_1 on temperature driven transition. Here $H_0 = 0.33pN$ (b) Effect of the cooperativity parameter H_1 on force driven transition. The simulation data represented by marker $\times$ is fit using the logistic function $g(x) = \frac{1}{1+e^{-a_0(x-a_1)}}$. Increasing the bending resistance of the base pairs leads to an increase in melting temperature and increases in the overstretching force. It also sharpens the force-driven transitions shown by the increasing values of a_0 as H_1 increases. The units of a_0 are K^{-1} in (a) and pN^{-1} in (b).

permittivity, and D is the dielectric constant of the solvent. c_0 is the concentration of monovalent ions, and $\chi^2 = \frac{2c_0e^2}{D\varepsilon_0 k_B T}$. The associated electrostatic energy E^{el} per unit length is obtained by incrementally charging the backbone from 0 to q[41]:

$$e^{el}(c_0, a+v_a) = -2k_BT\int_0^1 dt \;\; w(tq). \tag{31}$$

Note that the boundary condition on the average radius of the DNA backbone couples the electrostatic energy to the mechanical deformation of the birod. Hence, total energy per unit length $e(\theta(x), v(x))$ is the sum of the elastic (eqn.29) and electrostatic energy (eqn.31):

$$\begin{aligned} e(\theta(x), v(x)) =& EI(\theta_x^2 + v_{xx}^2) + (L_1 a^2 + \frac{F}{2})\theta^2 + \\ & L_2(e^{-\lambda v} - 1)^2 + H_1 v_x^2 - F v_x \theta + e^{el} \end{aligned} \tag{32}$$

Having set this up, we wish to compute effect of the ion concentration on the melting temperature and melting force. There is only one parameter in the entire electrostatic formulation: q. We choose $q = 0.05$ for the computations. We start by examining the effect of ion concentration on thermal melting. The fraction of melted DNA f_m versus the temperature T is computed for various concentrations $c_0 = 0.018$mol/L to 0.15 mol/L. The simulation results ($\times$) plotted in fig.7 (a) are fitted using a logistic function $f(x) = \frac{1}{1+e^{-a_0(x-a_1)}}$. The melting temperature is reached when $f_m \geq 0.5$. The simulations indicate that melting temperature T_m increases as the concentration c_0 increases as shown in fig.7(b). Next, we consider force-induced melting. The simulation data $\times$ and the respective logistic fits are shown in fig.7(c). We find that the melting force increases as the concentration increases, see fig.7(d). Previous works such as[8,40] have used thermodynamic analysis based on the Clausius-Clayperon equation together with experimental data to analyse the effect of concentration on thermal and force-induced melting and have reported similar results–the melting force and temperature increase with increasing ion concentration. In the analysis presented here the effect of ion concentration emerges from the coupling between the micromechanical deformations of the birod $v(x)$ and the Poisson-Boltzman electrostatic model of DNA. Although, we were able to account for the effect of electrostatics using an elementary Poisson-Boltzmann model, there are several drawbacks: i) the assumption that the rod is straight can not be true at force $F = 0$, ii) the Poisson-Boltzmann model works only for weak ionic

concentrations at $T << T_m$, iii) eqn.30 assumes that the positive ions are a non-interacting Boltzmann gas which is not true in the vicinity of DNA helix where ion-ion correlations must be considered and iv) eqn.30 neglects the effect of divalent ions such as Mg^{+2} and Ca^{+2}. For a detailed discussion, we refer the reader to the existing literature on solution electrostatics[41,42].

8 Conclusion

The theory of elastic birods is deployed to study temperature driven and tensile force driven melting transitions in DNA. The paper begins by discussing how the birod model embodies typical characteristics of entropic elasticity. Next, the model is used to study temperature induced DNA melting. The average inter-strand distance is found to increase monotonically with temperature in a nonlinear unbounded fashion. The nonlinear asymmetric interaction between the strands is crucial to correctly model the melting transition; for a linear-elastic interaction, leading to a quadratic energy functional, the average increase in the inter-strand distance is zero–independent of changes in temperature. Next, the model is used to study the effect of tensile force on the melting temperature. The model predicts that the melting temperature decreases with increasing tensile force and by appropriately choosing the elastic parameters the prediction can be shown to even match quantitatively with experimental data. The model shows that at a fixed temperature an increase in tensile load also leads to a melting transition and the critical force corresponding to this transition predicted by the model is 40 pN whereas the experimentally observed value is 60 pN. Various assumptions such as using a straight birod to model double-helical DNA and restricting to deformations on a plane could be responsible for the deviations. Furthermore, the birod model predicts that an increase in GC content causes an increase in cooperativity leading to higher melting temperature and melting forces. Finally, the interplay between the statistical mechanics of the birod model together with electrostatics from a Poisson-Boltzmann formulation accounts for the increase in melting temperatures and melting force with ion concentration.

This work demonstrates the ability of the elastic birod model to accurately describe the mechanics of the DNA melting transition in three ways: i) cooperativity in the melting transition, well documented in literature[4,8,16,17], emerges naturally from the elasticity of the base pairs, ii) the birod model can successfully account for the intertwined effect of temperature and tensile force on the melting transition, and iii) the model can be coupled to the Poisson-Boltzmann formulation to account for the effect of ion concentration. However, using a straight ladder-like birod to model double-helical DNA is at best a first order approximation. Such a model is unable to account for the 1.7 times stretching during the melting transition accomplished by unwinding the DNA helix. The derivation of the energy functional assumes that the change in inter-strand distance is small, however this is not true during the melting transition. Further study is required to examine the effect of nonlinear coupling terms in the model. In our formulation, the asymmetry in the applied force is responsible for coupling the stretch (θ) with the interstrand distance (v). As such, if equal force is applied on both ends the stretch and inter-strand distance are decoupled. However, this is because the DNA is modeled using a straight non-helical birod. The authors' previous work (see sec. 4 in supplementary materials[20]) on double-helical birods shows how the stretch is coupled to the inter-strand distance. Other crucial features of DNA arising out of double-helical topology, such as twist-stretch coupling, are absent in the straight ladder. Although, such a model can explain the melting transition, it can not explain other well documented[4,43] transitions among various DNA phases such B-DNA $\rightarrow$ S-DNA and B-DNA $\rightarrow$ P-DNA. Hence, a natural extension of this work is to study the statistical mechanics of a double-helical birod.

Conflicts of interest

There are no conflicts to declare.

Acknowledgement

JS and PKP acknowledge support for this work from grants NSF CMMI 1662101 and NIH R01 HL 135254. We thank the anonymous reviewers for pointing out several key points that helped us improve the manuscript.

Appendix

A1: A simple model illustrating cooperativity

The concept and effects of cooperativity are demonstrated using an elastic bar under a tensile load. The understanding derived from this exercise helps us rationalize the observations reported in the main text. Let the strain variable be $v(x)$, hence the energy functional of the bar under a tensile load is $E = \int_0^L dx \frac{v^2}{2} - F\Delta$, where L is the contour length and Δ is the displacement at the free end which can be expressed an an integral over the strain– $\Delta = \int_0^L v dx$. Now, we add a cooperativity term proportional to v_x^2. This is analogous to the surface energy term in the Allen-Cahn energy functional[44] and gradient term in Landau-Ginzburg energy functional[12]. In view of the above discussion, the energy functional is,

$$E = \int_0^L dx \Big(k \frac{v_x^2}{2} + \frac{v^2}{2} - F v \Big). \tag{33}$$

To get the $\langle v \rangle$ vs F curve for the bar, we have:

$$\langle v \rangle = \frac{1}{Z} \int \mathscr{D}v(x) \Big(\frac{1}{L} \int_0^L v(x) dx \Big) \exp\big(- \frac{E(v(x))}{k_B T} \big) \tag{34}$$

where $Z = \int \mathscr{D}v(x) \exp\big(- \frac{E(v(x))}{k_B T} \big)$ is the partition function. Similarly, $\langle v \rangle$ vs T curves can also be obtained.

For simplicity, assume $v(x)$ can either be relaxed or stretched: $v \in \{0, 1\}$. Using the assumption, together with techniques used in the main text to numerically evaluate the partition function, we can compute the $\langle v \rangle$ vs F and $\langle v \rangle$ vs T curves. We focus on the effect of the cooperativity parameter k on the curves. The results are shown in fig.9. Fig.9 (a) shows that for a fixed temperature T, $\langle v \rangle$ decreases with an increase in the cooperativity parameter k, a

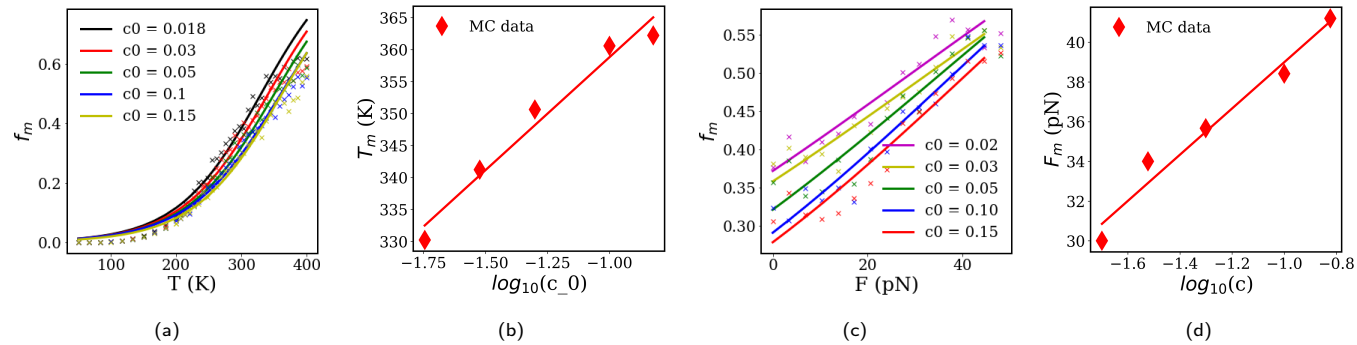

Fig. 7 Effect of ion concentration (a) Fraction of melted DNA f_m versus the temperature T for various ion concentration, $F = 0$ (b) Monotonically increase in melting temperature T_m with the ion concentration c_0. (c) Fraction of melted DNA $f_m$versus the applied tensile load F, $T = 300$K. (d) Monotonically increasing melting force F_m with the ion concentration c_0.

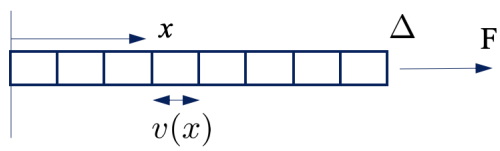

Fig. 8 An elastic bar undergoing a cooperative phase transition. Here $v(x)$ is the strain variable.

similar trend is observed by increasing H_1 as shown in fig. 6(a) of the main text. Regarding the force driven stretching, fig. 9(b) shows that the width of the transition decreases with increasing k: $\langle v \rangle$ vs F curve is almost linear for $k = 0$ while for $k = 3.0$ it is sigmoidal. This happens because for large cooperativity coefficient $k = 3.0$, the units stretch simultaneously. To illustrate this point, we present the stretched and unstretched units in fig.10 for values of F below and above the melting force ($F = 0.8, 1.2$) using cooperativity parameters $k = 0$ and $k = 3.0$. Similar sharpening of transition is also observed by increasing H_1 in fig. 6(b) of the main text. While in this simple model, the sharpening effect of cooperativity can be clearly seen as shown in fig.9(b), and fig.10, in sec.6, we need to fit logistic curves to the MC simulation data to quantify the sharpness. One point of departure between the two models, is that the melting force increases with H_1 in fig. 6(b), on the other hand it remains constant with increasing k in fig.9(b). This is because in the main text, the work done by the external force F is proportional to $F v_x \theta$ and θ decreases as F increases, consequently a larger force is required to melt the DNA. Based upon these two similarities, we claim that H_1 is the cooperativity parameter in the birod model in the main text.

A2: Analytical derivation of the force-extension curve

Here, we use Fourier integral techniques* to get an analytical expression for the force-extension curve[30,31]. The energy functional in sec.3 is,

$$E = \int_x dx \Big(EI\theta_x^2 + (\frac{F}{2} + L_1 a^2)\theta^2 \Big). \tag{35}$$

Define,

$$\tilde{\theta}(q) = \frac{1}{2\pi} \int_x dx e^{-iqx} \theta(x) \quad \text{and} \quad \theta(x) = \int_q dq e^{iqx} \theta(q). \tag{36}$$

Noting that $\theta(x)^2 = \int_q \int_q dq_1 dq_2 e^{iq_1 x} e^{-iq_2 x} \tilde{\theta}(q_1)\tilde{\theta}(q_2)$ and $\int_x dx e^{i(q_1 - q_2)x} = \delta_{q_1 - q_2}$ into eqn.35, we get,

$$E = \int_q dq \Big(EIq^2 + (\frac{F}{2} + L_1 a^2) \Big) \tilde{\theta}^2. \tag{37}$$

The above expression is quadratic in $\tilde{\theta}(q)$, hence, using equipartition one can evaluate

$$\langle \tilde{\theta}(q)^2 \rangle = \frac{k_B T}{EIq^2 + (\frac{F}{2} + L_1 a^2)}. \tag{38}$$

Parseval's identity–$\int_x \theta(x)^2 dx = \frac{1}{2\pi} \int_q \tilde{\theta}(q)^2 dq$–together with the above equation yield the following expression for the average end-to-end distance:

$$< y > = L \Big(1 - \frac{k_B T}{8\sqrt{EI(F/2 + L_1 a^2)}} \Big). \tag{39}$$

In the limit $F >> L_1 a^2$, the persistence length ℓ_p can be obtained by comparing the above expression to the WLC formula ($\langle y \rangle = L - \frac{L}{2}\sqrt{\frac{k_B T}{F \ell_p}}$): $\ell_p = \frac{8EI}{k_B T}$. We verify this assumption by performing a simple calculation shown in fig.11. We can not do this calculation in sec. 3 to obtain the persistence length because the assumption $F >> L_1 a^2$ does not hold true, instead $F \sim L_1 a^2$. For a similar calculation of $\langle w^2(x) \rangle$, we direct the reader to Purohit *et al.*[31].

A3: Details of MC simulations

The Monte Carlo simulations were performed using the Metropolis-Hastings algorithm[35]. The DNA oligomer was modeled using a 2D birod fixed on one end and free on the other as shown in fig.1 of the main text. The length of oligomers was $L = 40$ nm and was discretized into $n = 50$ elements which gives

* We thank a reviewer for this suggestion.

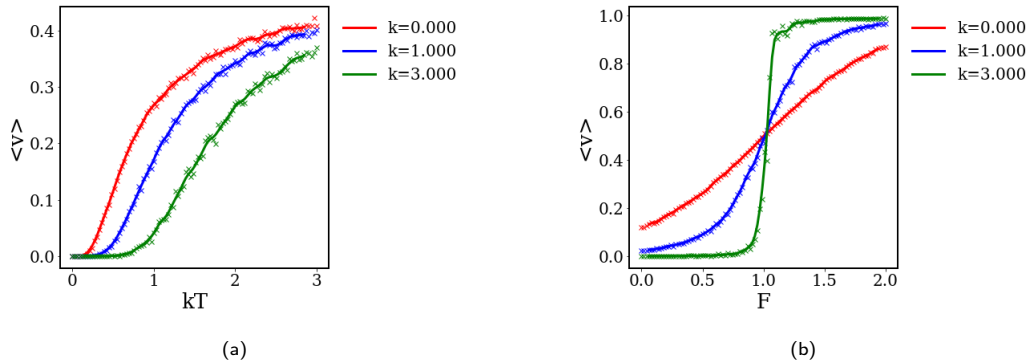

Fig. 9 Here $\times$ are the MC simulations while the solid lines are the smoothed spline being fit to the MC simulation data. (a) $\langle v \rangle$ vs T curves at $F = 0$, (b) $\langle v \rangle$ vs F curves at $k_B T = 0.5$.

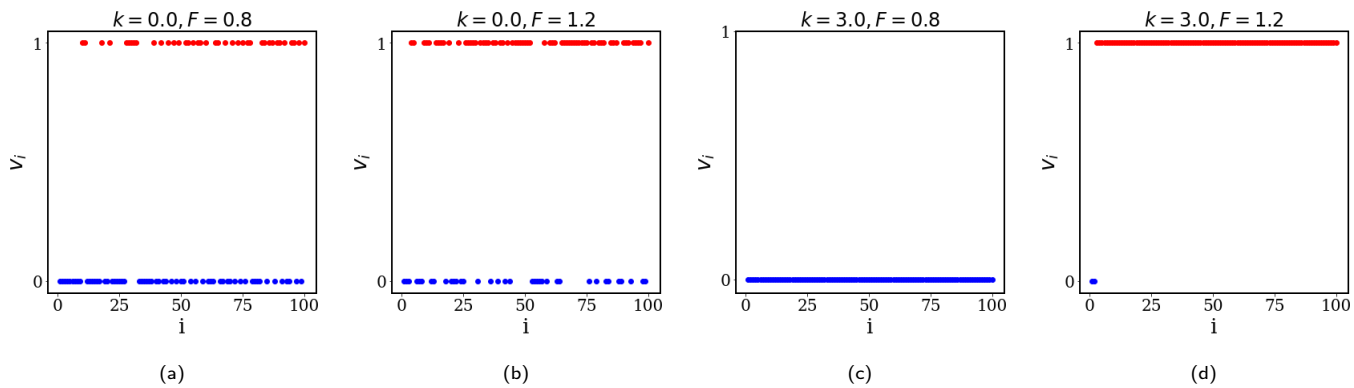

Fig. 10 Here $\circ$ denotes melted $(=1)$ or unmelted $(=0)$ state of ith unit at the end of the simulation ($N = 100000$ steps). We see a sudden transition from $F = 0.8$ to $F = 1.2$ when the cooperativity parameter is large ($k = 3$) in (c) and (d), respectively. On the other hand, we see smooth cross over when cooperativity parameter is low ($k = 0$). The values of k and F are given in the figure titles and $k_B T = 0.5$.

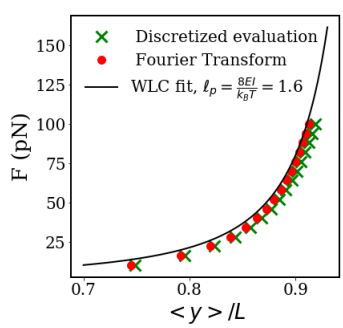

Fig. 11 Using $k_B T = 5$, $L_1 = 1$, $EI = 1$, and $L = 10$. Here $\times$ data is obtained by discretizing the birod into $n = 100$ elements.

$m = 100$ dof: (θ_i, v_i) $0 \le i < n$. The total number of MC moves was $N = 1000000$. At each move, a random degree of freedom was chosen and the magnitude of perturbation was normally distributed with mean 0 and standard deviation σ_v if the chosen dof is v_i and σ_θ if the chosen dof is θ_i. The perturbed state is accepted if $e^{-\frac{\Delta E}{k_B T}} > \alpha$, where ΔE is the energy difference between the initial state and perturbed ($\Delta E = E_{\text{perturbed}} - E_{\text{initial}}$) and α is a random floating point number uniformly distributed between 0 and 1 ($\alpha \sim U(0,1)$). We checked for the saturation of the energy to ensure steady-state. The averages were computed on the last $N/2$ states to discount the effects of burn-in process. The values of σ_v (≈ 0.25 nm) and σ_θ (≈ 0.2) were chosen such that the accepted fraction of states lies between $20 - 40\%$. The melted fraction $f_m = \frac{1}{n}\sum_{i=1}^{n} \mathbb{I}(v_i > 5\text{Å})$, where $\mathbb{I}(v_i > 5\text{Å}) = 1$ if $v_i > 5\text{Å}$ and 0 otherwise. The DNA oligomer is considered melted when $f_m > 0.5$. For $f_m = 0.5$, we will always have $\langle v \rangle > 5\text{Å}$, since there will be melted links where $v_i > 10\text{Å}$, while for unmelted units $0 < v_i < 5\text{Å}$.

To access the impact of concentration, we need to compute the electrostatic free energy per unit length $E^{el}(a + v_a)$ as a function of the average birod radius $a + v_a$. Note that v_a changes with each MC move, and solving the ODE at each move is computationally expensive. To circumvent the issue, $E^{el}(a + v_a)$ was computed for various values of $a + v_a$ and an exponential curve was fit to the data. The fitted exponential curve was then used to compute E^{el} in the MC simulations. For reference, we show E^{el} vs $a + v_a$ and the fitted exponential curve for solution concentration $c_0 = 0.1$M and $T = 300$K in fig.12.

A4: Effect of increasing GC content

In sec.6, the effect of the cooperativity parameter H_1 is discussed. It was observed that the melting temperature increases with increase in the value of H_1, which in turn, is due to higher GC content. Higher GC content can have many other effects as well, such as higher stretch moduli L_1 and shear moduli L_2, and the

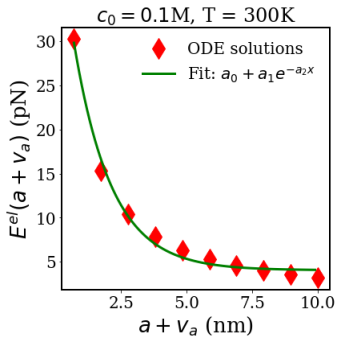

Fig. 12 Plot of E^{el} vs $a + v_a$. The fitted exponential curve is used to compute E^{el} in MC simulations.

combined inter-play could be much more complex and beyond the scope of the paper. Since, the section focusses on the effect of cooperativity, we increased only H_1 and left L_1 and L_2 unchanged. Here we change all the parameters H_1, L_1 and L_2 and show similar trends.

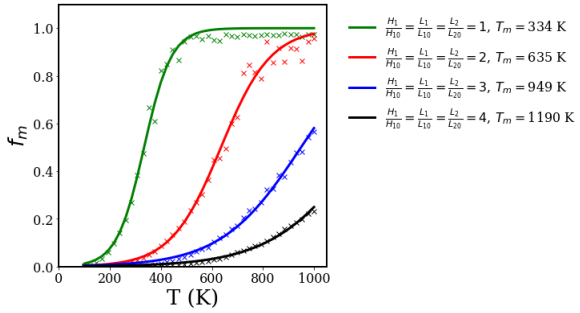

Fig. 13 Fraction of melted DNA f_m vs temperature T. Here, instead of changing only H_1, we change all the parameters L_1,L_2 and H_1. As the stiffness of the base pairs increases, the melting temperature T_m increases.

References

1 C. Giardina and J. T. Lis, *Science*, 1993, **261**, 759–762.

2 B. Rad, A. L. Forget, R. J. Baskin and S. C. Kowalczykowski, *Proceedings of the National Academy of Sciences*, 2015, **112**, E6852–E6861.

3 R. M. Brosh Jr, *Nature Reviews Cancer*, 2013, **13**, 542–558.

4 X. Zhang, H. Chen, H. Fu, P. S. Doyle and J. Yan, *Proceedings of the National Academy of Sciences*, 2012, **109**, 8103–8108.

5 G. A. King, E. J. Peterman and G. J. Wuite, *Nature communications*, 2016, **7(1)**, 1–7.

6 G. A. King, P. Gross, U. Bockelmann, M. Modesti, G. J. Wuite and E. J. Peterman, *Proceedings of the National Academy of Sciences*, 2013, **110**, 3859–3864.

7 M. C. Williams, J. R. Wenner, I. Rouzina and V. A. Bloomfield, *Biophysical Journal*, 2001, **80**, 874–881.

8 I. Rouzina and V. A. Bloomfield, *Biophysical journal*, 2001, **80**, 894–900.

9 J. M. Gibbs-Davis, G. C. Schatz and S. T. Nguyen, *Journal of the American Chemical Society*, 2007, **129**, 15535–15540.

10 K. Nishigaki, Y. Husimi, M. Masuda, K. Kaneko and T. Tanaka, *The Journal of Biochemistry*, 1984, **95**, 627–635.

11 M. Moakher and J. Maddocks, *Archive for rational mechanics and analysis*, 2005, **177**, 53–91.

12 L. D. Landau and E. M. Lifshitz, *Statistical Physics: Volume 5*, Elsevier, 2013, vol. 5.

13 G. Lehman and J. McTague, *The Journal of Chemical Physics*, 1968, **49**, 3170–3179.

14 D. M. Crothers, *Biopolymers: Original Research on Biomolecules*, 1968, **6**, 1391–1404.

15 I. Rouzina and V. A. Bloomfield, *Biophysical journal*, 2001, **80**, 882–893.

16 T. Dauxois, M. Peyrard and A. R. Bishop, *Physical Review E*, 1993, **47**, R44.

17 M. Peyrard and A. R. Bishop, *Physical review letters*, 1989, **62**, 2755.

18 A. Pérez, F. J. Luque and M. Orozco, *Accounts of chemical research*, 2012, **45**, 196–205.

19 F. Zhang and M. A. Collins, *Physical Review E*, 1995, **52**, 4217.

20 J. Singh and P. K. Purohit, *Proceedings of the Royal Society A: Mathematical, Physical and Engineering Sciences*, 2018, **474**, 20180136.

21 J. Singh and P. K. Purohit, *The Journal of Physical Chemistry B*, 2018, **123**, 21–28.

22 E. H. Dill, *Archive for History of Exact Sciences*, 1992, **44**, 1–23.

23 D. Argudo and P. K. Purohit, *Journal of the Mechanics and Physics of Solids*, 2014, **62**, 228–256.

24 A. Marantan and L. Mahadevan, *American Journal of Physics*, 2018, **86**, 86–94.

25 R. S. Manning, J. H. Maddocks and J. D. Kahn, *The Journal of chemical physics*, 1996, **105**, 5626–5646.

26 D. Petkeviciute, *A DNA coarse-grain rigid base model and parameter estimation from molecular dynamics simulations*, Epfl technical report, 2012.

27 T. Dršata, M. Zgarbová, P. Jurečka, J. Šponer and F. Lankaš, *Biophysical journal*, 2016, **110**, 874–876.

28 X. Xu, H. Ge, C. Gu, Y. Q. Gao, S. S. Wang, B. J. R. Thio, J. T. Hynes, X. S. Xie and J. Cao, *The Journal of Physical Chemistry B*, 2013, **117**, 13378–13387.

29 T. Su and P. K. Purohit, *Journal of the Mechanics and Physics of Solids*, 2010, **58**, 164–186.

30 J. F. Marko and E. D. Siggia, *Macromolecules*, 1995, **28**, 8759–8770.

31 P. K. Purohit, M. E. Arsenault, Y. Goldman and H. H. Bau, *International Journal of Non-Linear Mechanics*, 2008, **43**, 1056–1063.

32 J. F. Marko and E. D. Siggia, *Macromolecules*, 1995, **28**, 8759–8770.

33 I. Rouzina and V. A. Bloomfield, *Biophysical journal*, 1999, **77**, 3252–3255.

34 R. Blake and S. G. Delcourt, *Nucleic acids research*, 1998, **26**, 3323–3332.

35 R. Pathria and P. D. Beale, *Statistical mechanics*, Butter worth, 1996, vol. 32.

36 P.-G. de Gennes, *arXiv preprint physics/0110011*, 2001.

37 X. Zhang, H. Chen, S. Le, I. Rouzina, P. S. Doyle and J. Yan, *Proceedings of the National Academy of Sciences*, 2013, **110**, 3865–3870.

38 J. Singh and P. K. Purohit, *Acta biomaterialia*, 2017, **55**, 214–225.

39 R. Phillips and P. Rob, *Crystals, defects and microstructures: modeling across scales*, Cambridge University Press, 2001.

40 J. R. Wenner, M. C. Williams, I. Rouzina and V. A. Bloomfield, *Biophysical journal*, 2002, **82**, 3160–3169.

41 M. Frank-Kamenetskii, V. Anshelevich and A. Lukashin, *Soviet Physics Uspekhi*, 1987, **30**, 317.

42 D. R. Jacobson and O. A. Saleh, *Nucleic acids research*, 2017, **45**, 1596–1605.

43 A. Sarkar, J.-F. Leger, D. Chatenay and J. F. Marko, *Physical Review E*, 2001, **63**, 051903.

44 R. Phillips and P. Rob, *Crystals, defects and microstructures: modeling across scales*, Cambridge University Press, 2001.

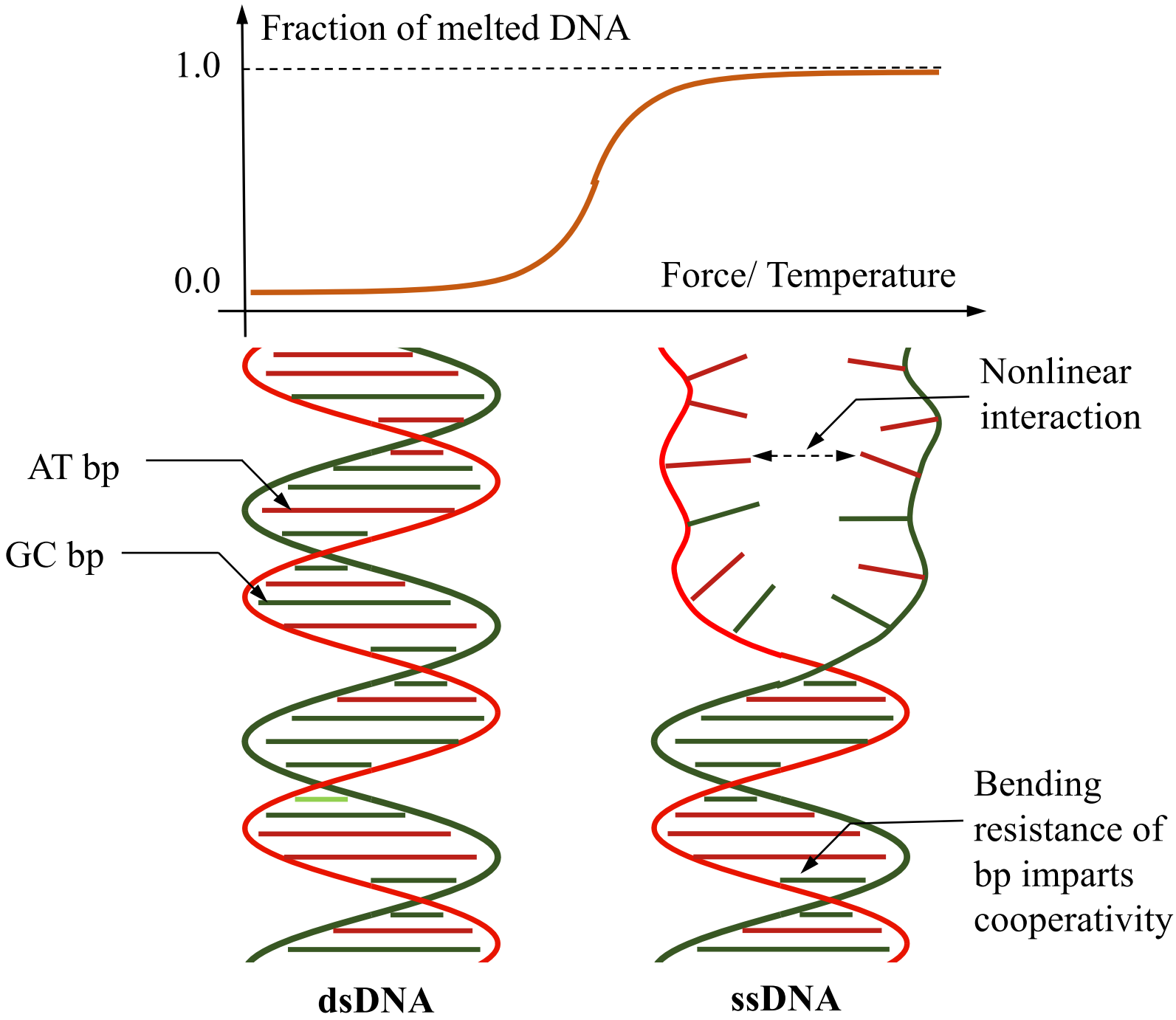
Fraction of melted DNA
1.0
0.0
Force/ Temperature
AT bp
GC bp
Nonlinear interaction
Bending resistance of bp imparts cooperativity
dsDNA
ssDNA